

Current amplification and magnetic reconnection at a 3D null point. I - Physical characteristics

D. I. Pontin*

*Space Science Center, University of New Hampshire, USA
(now at Department of Mathematics, University of Dundee, Dundee, Scotland)*

K. Galsgaard

Niels Bohr Institute, University of Copenhagen, Copenhagen, Denmark

The behaviour of magnetic perturbations of an initially potential three-dimensional equilibrium magnetic null point are investigated. The basic components which constitute a typical disturbance are taken to be rotations and shears, in line with previous work. The spine and fan of the null point (the field lines which asymptotically approach or recede from the null) are subjected to such rotational and shear perturbations, using three-dimensional magnetohydrodynamic simulations. It is found that rotations of the fan plane and about the spine lead to current sheets which are spatially diffuse in at least one direction, and form in the locations of the spine and fan. However, shearing perturbations lead to 3D-localised current sheets focused at the null point itself. In addition, rotations are associated with a growth of current parallel to the spine, driving rotational flows and a type of rotational reconnection. Shears, on the other hand, cause a current through the null which is parallel to the fan plane, and are associated with stagnation-type flows and field line reconnection across both the spine and fan. The importance of the parallel electric field, and its meaning as a reconnection rate, are discussed.

I. INTRODUCTION

Many important physical phenomena in astrophysical plasmas are powered by magnetic reconnection. The locations at which reconnection is likely to occur in a complex three-dimensional magnetic field are those regions where strong currents (possibly singular in the ideal regime) may develop. However, determining what these locations might be is a non-trivial problem.

There are a growing number of theories and pieces of evidence to suggest that 3D null points and separators (magnetic field lines which join two such nulls) may be sites of preferential current growth, in both the Solar corona and the Earth's magnetosphere. The field topology in the vicinity of such a 3D null point is defined by the field lines which asymptotically approach (or recede from) the null. These fall into two categories. A single pair of field lines approach (recede from) the null from opposite directions, and are termed the 'spine' (or γ -line), while an infinite family of field lines recede from (approach) the null in a surface called the fan (or Σ -) plane. The spine and fan of a given null may be determined by examining the linear field topology near the null, defined by the equation

$$\mathbf{B} = \mathcal{M} \cdot \mathbf{r},$$

where the matrix \mathcal{M} is given by the Jacobian of \mathbf{B} [e.g. 10]. The eigenvectors of \mathcal{M} (whose corresponding eigenvalues sum to zero since $\nabla \cdot \mathbf{B} = 0$) now define the spine and fan. The two eigenvectors whose eigenvalues are of

like sign (or whose real parts have like sign) lie in the fan plane, while the third points along the spine. The fan surface is a separatrix surface of the magnetic field, separating unique topological regions. While the spine does not separate topological regions (being only a line), it is nonetheless an important geometrical feature of the field. This is because, firstly, magnetic field lines converge on (or diverge from) it, and secondly, it is a field line along which disturbances may be channelled towards the null (as we shall see later).

3D null points are predicted to be present in abundance in the solar corona. It should however be noted that many recent models of the magnetic field above the solar surface are based upon the Magnetic Charge Topology approach, extrapolating a potential field from point magnetic sources in the photosphere. This is clearly a great simplification, and many (or all) of the 'photospheric null points' in such models will not be present when these idealised flux sources are replaced by more realistic finite flux patches. However, various approaches also predict the presence of 3D null points up in the corona, with an average of between approximately 7 and 15 coronal nulls expected for every 100 photospheric flux concentrations [4, 18, 31]. The presence of these coronal nulls is expected to be more robust to the method of field extrapolation [1, 2]. The separatrix surfaces and separators associated with these coronal null points are thought to be likely sites of coronal heating and reconnection [17, 27]. Furthermore, there is observational evidence that reconnection at a 3D null point (both fan-type and spine-type reconnection) may be at work in some solar flares [9]. Closer to home, separator reconnection is thought to occur on the dayside of the Earth's magnetosphere [e.g. 32]. In addition, there has been a recent in situ observation by the Cluster spacecraft [33] of a 3D magnetic null, at

*Electronic address: dpontin@maths.dundee.ac.uk

which it is proposed that reconnection is occurring, located within the current sheet in the Earth's magnetotail.

Although it is now realised that 3D nulls are of great importance for reconnection in realistic 3D geometries, what is still lacking is a clear picture of what reconnection processes at such nulls look like. In particular, a description of the sorts of physical signatures expected (current sheets, plasma flows etc.), in order to lead the analysis of new observations, is of great importance. Our aim in this paper is to go some way to providing such a picture.

While the relationship between reconnection at a separator and a single 3D null point is not well known, it is clear that the two should be linked in some way. What is known is that both are prone to collapse in response to external motions [e.g. 3, 19, 22]. That is, a 3D null point is a 'weak point' of the magnetic field to which disturbances are attracted [11, 13]. Furthermore, kinematic considerations suggest that null points and separators are both locations where singularities may form in ideal MHD [e.g. 16, 28]. The attraction of disturbances to 2D nulls is also well documented [e.g. 8, 14].

The local behaviour of a perturbed 3D magnetic null point has been examined in the linear regime for the cold, resistive MHD equations by [29]. They employed a modal decomposition, and determined that only $m = 0$ and $m = 1$ modes can lead to currents at the null point, where m is the azimuthal wavenumber. In addition, they found that while $m = 0$ modes are attracted to the spine and fan of the null, $m = 1$ type perturbations tend to focus in towards the null itself. This was demonstrated in the linear regime with 2D simulations in the rz -plane. One of the major aims of the present work is to ascertain whether such behaviour for the evolution of disturbances is found in the full MHD regime, using 3D simulations.

In addition to the above, we will investigate which current components develop at the null in response to different perturbations, and the implications which this has for the plasma flow and field line behaviour. In each case we consider, the plasma is initially at rest, and so with no flow through our boundaries, we do not compare with strongly driven flux pile-up models [e.g. 5]. It is anticipated that different current orientations at the null will lead to very different behaviour [24, 25]. One of the present simulations is very similar to that described in the work of [12], and so is only briefly summarised in what follows. The other simulations combine with this to create a complete picture of the subject at hand.

In Section II we describe the numerical scheme and the initial conditions used. In Sections III–VI we describe the results of our simulations for various different types of perturbations, and in Section VII we give a summary and conclusions.

II. NUMERICAL SCHEME AND SIMULATION SETUP

A. Numerical Scheme

The numerical scheme employed in the simulations which follow is described briefly below (further details may be found in [21] and at <http://www.astro.ku.dk/~kg>). We solve the three-dimensional resistive MHD equations in the form

$$\frac{\partial \mathbf{B}}{\partial t} = -\nabla \times \mathbf{E}, \quad (1)$$

$$\mathbf{E} = -(\mathbf{v} \times \mathbf{B}) + \eta \mathbf{J}, \quad (2)$$

$$\mathbf{J} = \nabla \times \mathbf{B}, \quad (3)$$

$$\frac{\partial \rho}{\partial t} = -\nabla \cdot (\rho \mathbf{v}), \quad (4)$$

$$\frac{\partial}{\partial t} (\rho \mathbf{v}) = -\nabla \cdot (\rho \mathbf{v} \mathbf{v} + \underline{\underline{\tau}}) - \nabla P + \mathbf{J} \times \mathbf{B}, \quad (5)$$

$$\frac{\partial e}{\partial t} = -\nabla \cdot (e \mathbf{v}) - P \nabla \cdot \mathbf{v} + Q_{visc} + Q_J, \quad (6)$$

where \mathbf{B} is the magnetic field, \mathbf{E} the electric field, \mathbf{v} the plasma velocity, η the resistivity, \mathbf{J} the electric current, ρ the density, $\underline{\underline{\tau}}$ the viscous stress tensor, P the pressure, e the internal energy, Q_{visc} the viscous dissipation and Q_J the Joule dissipation. An ideal gas is assumed, and hence $P = (\gamma - 1) e = \frac{2}{3} e$.

The equations above have been non-dimensionalised by setting the magnetic permeability $\mu_0 = 1$, and the gas constant (\mathcal{R}) equal to the mean molecular weight (M). The result is that, for a cubic domain of unit size, if $|\rho| = |\mathbf{B}| = 1$, then time is measured in units of the Alfvén travel time across the domain ($\tau_A = L\sqrt{\mu\rho_0}/B_0$, where L is the size of the domain, and ρ_0 and B_0 are typical values of the density and magnetic field respectively).

The equations are solved on staggered meshes; in this way the required MHD conservation laws are automatically satisfied. Spatial derivatives are evaluated using a sixth-order-accurate finite difference method. It is often the case that, due to the staggered mesh, this value of the derivative is returned in exactly the position it is needed. When this is not the case, the values are calculated using a fifth-order interpolation method at the relevant position. A non-uniform mesh is used in the simulations, with higher resolution in the centre of the domain in each coordinate direction. In this way it is possible to better resolve behaviour in the vicinity of the null, and indeed across the spine and fan, while keeping the boundaries 'far away' to reduce their effect. A third-order predictor-corrector method is employed for time-stepping. All simulations are carried out on grids of 128^3 or 256^3 resolution.

Viscosity is handled using a combined second-order (constant ν) and fourth-order method, which is capable of providing sufficient localised dissipation where necessary to handle the development of numerical instabilities. The result is that it is possible to achieve much

lower effective values of ν for a given numerical resolution than with a constant- ν approach. This is achieved by having an enhanced viscosity at length scales close to the numerical resolution limit, effectively dissipating short wavelength disturbances, while leaving larger-scale structures nearly undamped. Viscosity defined in such a way is often termed ‘hyper-viscosity’. Such an approach is used in 3D simulations to maximise the fraction of the 3D domain that has an ‘ideal’ behaviour. Two different models are used for the resistivity; either a traditional constant- η (second-order) model or a hyper-resistivity model (labelled η_h in the text) similar in approach as the viscosity model. Comparisons between identical simulation runs using the two resistivity approaches show the same general evolution, with the main difference being that the hyper-resistivity runs show more spacially localised structures. This is demonstrated explicitly for one particular case below (see Section V).

In a number of the simulation runs, ‘trace particles’ are used in order to track the motion of field lines in time. These points are chosen at $t = 0$, and are then followed in time throughout the simulation by integrating the plasma flow field. These ‘fluid elements’ are then used to define field line footprints.

Finally, the boundary conditions are closed in all three directions. In addition, as we aim to study only the initial localisation of perturbations at the null, a boundary damping zone is included, in order to limit the reflection of waves back into the domain from the boundary. Within this region, a fraction of the kinetic energy is removed per unit time, which, when chosen appropriately for the wave speed, may effectively damp a large portion of the wave energy. The effect of the boundaries on the dynamics of the null point is, on the other hand, negligible, as the simulations are all terminated before the perturbations have time to reflect off them and reach back to the region around the null again.

B. Initial setup

The simulation is set up as follows. The initial ‘background’ magnetic field is potential, and describes a 3D magnetic null point located at the origin, specifically $\mathbf{B} = B_0(x, y, -2z)$. The plasma is initially at rest, with $\rho = 1$, $e = 5\beta/2$ everywhere, where β determines the plasma- β . The system is then disturbed by perturbing the magnetic field. We choose to add a magnetic field instead of, say, imposing some velocity on a line-tied boundary, so as to examine the evolution of the null point, and the reconnective behaviour, in an undriven situation. We focus on the behaviour of the transient pulse as it moves towards the null. Note that the fact that there is no flow through our boundaries means that we do not compare with strongly driven flux pile-up models.

In order for the null point to be affected, the perturbation must disturb either the spine or fan of the null, otherwise the disturbance will simply propagate back and

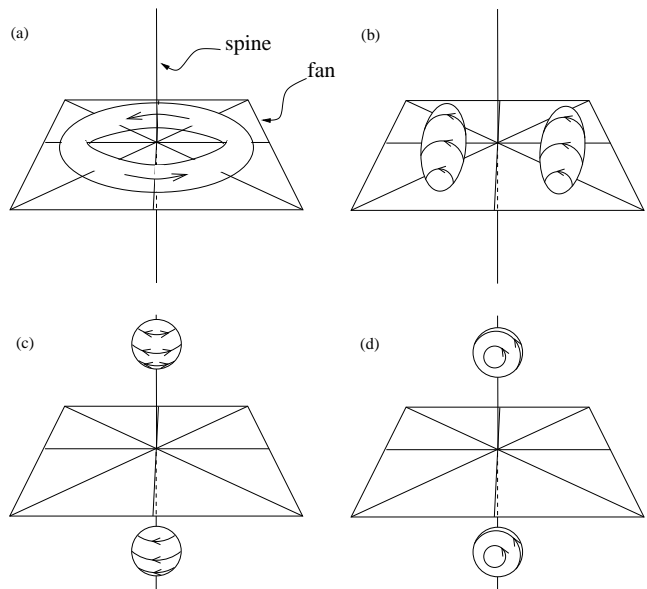


FIG. 1: Schematic view of isosurfaces of the different perturbation magnetic fields, with arrows indicating the field orientation. (a) rotation within the fan plane, (b) shear in the fan plane (c) rotation of the spine, in the same or opposite sense above and below the fan, and (d) shear of the spine. In each case the vertical line is the (undisturbed) spine of the null, and the square is the fan.

forth along the associated magnetic field lines, bouncing between the boundaries. The perturbation magnetic field must of course be divergence-free, and in each of the cases discussed takes the general form

$$\begin{aligned} b_i &= -b_0 R_1 \sin(\theta_1) \exp\left(-\frac{(R_1 - R_{10})^2}{a_h^2} - \frac{(\zeta - \zeta_0)^2}{b_h^2}\right) \\ b_j &= b_0 R_1 \cos(\theta_1) \exp\left(-\frac{(R_1 - R_{10})^2}{a_h^2} - \frac{(\zeta - \zeta_0)^2}{b_h^2}\right), \end{aligned} \quad (7)$$

where b_i and b_j are the two components of the perturbation magnetic field, ζ is the third spatial coordinate, and b_0 , R_{10} , ζ_0 , a_h and b_h are constants. R_1 and θ_1 are defined depending on the orientation of the perturbation. The perturbation is localised by the exponential terms within either a linear tube or a torus.

Five different types of perturbation will be considered. These are described briefly below, and are illustrated in Figures 1 and 2. Figure 1 shows isosurfaces of the disturbance field magnitude, with the arrows showing the direction of the field. Figure 2 plots a selection of field lines from around the null, showing the effect of the disturbances on the the magnetic field. The first type of perturbation corresponds to the $m = 0$ disturbances of [29], that is, rotational motions. We consider two cases, in the first of which (Section III) the rotation is concentrated in the fan plane (but away from the null, see Figures 1(a), 2(a)). One may also perform a rotation about the spine, but away from the fan plane, either in the same or opposite sense above and below the fan (see Figures 1(c), 2(c)). This has been investigated in detail

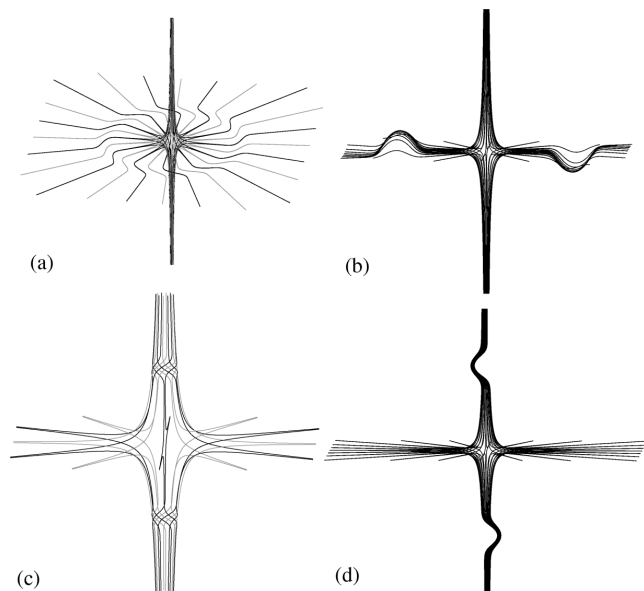


FIG. 2: Sample magnetic field lines at $t = 0$ for the different perturbations, (a)-(d) as in Figure 1.

by [12], and is discussed briefly in Section IV. Alternatively, the null point separatrices may be perturbed by applying some shear (corresponding to $m = 1$), to either the fan (Section V, Figures 1(b), 2(b)) or the spine (Section VI, Figures 1(d), 2(d)). Any more generic perturbation may be made up from a combination of such rotations and shears.

III. ROTATION IN THE FAN PLANE

For a rotation in the fan plane, the perturbation magnetic field lies in the xy -plane, such that $\{b_i, b_j\} = \{b_x, b_y\}$ and $\zeta = z$ in Equation (7), and in addition we take $R_1 = \sqrt{x^2 + y^2}$, $\theta_1 = \tan^{-1}(y/x)$, and $\zeta_0 = 0$. Thus the current is initially concentrated in a torus whose toroidal axis lies in the fan plane at a radius R_{10} from the origin (null), see Figures 1(a) and 2(a). The domain size is chosen to be $1.5 \times 1.5 \times 2.5$, in order to limit the effect of the upper/lower boundaries in z . We use the hyper-resistive model, $\eta = \eta_h$, and the characteristic parameters for the experiment are; $B_0 = 1, b_0 = 0.1, R_{10} = 0.16, \beta = 0.01, a_h = b_h = 0.06$, giving a travel time to the top (z) boundary of order 1.8 and to the xy -boundaries of 1.5 in code units, for the main body of the disturbance.

A. Current density evolution

Figure 3 shows the time evolution of the current modulus in a plane through the null and spine axis (chosen to be the $y = 0$ plane, although we have cylindrical symmetry away from the boundaries). It is evident from the image that pulses propagating both inwards and out-

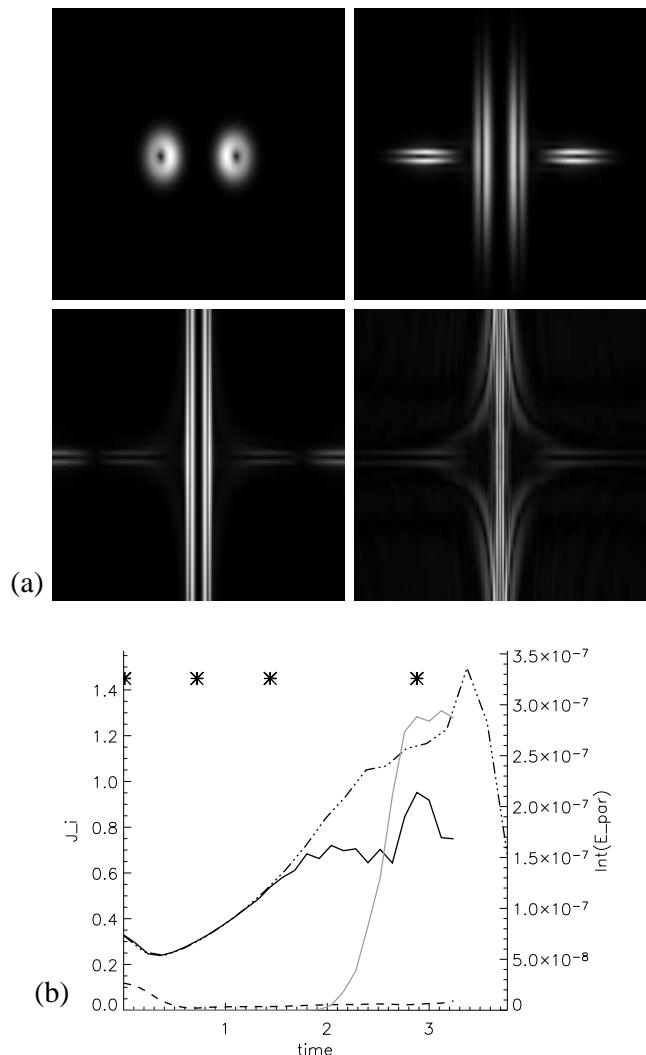


FIG. 3: For a rotation of the fan; (a) current modulus in the $y = 0$ plane for $[x, z] = [\pm 0.75, \pm 0.75]$, at times marked by asterisks in (b) ($t = 0, 0.72, 1.44, 2.88$). (b) Evolution of the maximum value of each current component (J_x and J_y dashed, J_z solid, black) and of the integrated parallel electric field along the spine (grey). Domain size is $1.5 \times 1.5 \times 2.5$ and parameters used are $B_0 = 1, b_0 = 0.1, R_{10} = 0.16, \beta = 0.01, a_h = 0.06, b_h = 0.06$ and $\eta = \eta_h$. The dot-dashed line shows J_z evolution in a run with the same parameters, but at 256^3 resolution.

wards develop, as one would expect. In the following, we refer to the disturbances which propagate towards and away from the null point as the ‘ingoing’ and ‘outgoing’ pulses, respectively. Note that here, as in the simulations which follow, both the ingoing pulse and outgoing pulse have a somewhat complicated structure. Specifically, it appears from Figure 3(a) that there are two wavefronts which localise towards the null, although in fact these two wavefronts (in $|\mathbf{J}|$) correspond to current concentrations of opposite sign (in J_z), which demark strong field gradients at the ‘back end’ and ‘front end’ of the single

ingoing ‘pulse’. The magnetic field gradients must necessarily pass through zero at the centre of this pulse, hence the appearance of two strong bands in $|\mathbf{J}|$. The ingoing pulse propagates along the ‘background’ field lines, and concentrates in a current tube centred on the spine. There is, however, no preferential attraction of the current to the null itself. It is interesting that even though the field structure is hyperbolic, the current localises very uniformly in z , i.e. the wavefront is very close to vertical, as would be expected for an Alfvén wave. Note finally that in the last image there are some unavoidable reflections of the disturbance from the upper boundary back along the background field lines. We have checked that the boundaries play no significant role in the qualitative or quantitative evolution by repeating the simulation in a domain of dimensions $1.5 \times 1.5 \times 4.5$ (which increases the perturbation travel time to and from the z -boundaries to greater than 4 in code units).

Further insight may be gained by examining the evolution of the different components of the current. The maximum value of each component is plotted in Figure 3(b) (we take the maximum within the region $[\pm 0.25, \pm 0.25, \pm 0.42]$ in each direction to exclude boundary effects). The figure shows that as the current localises towards the spine, it is J_z , i.e. the current parallel to the spine, which is significantly amplified, while J_x and J_y are not. This is to be expected, as it is dx and dy which are decreasing as the disturbance is squeezed in towards the spine. The current eventually reaches a maximum as it localises. This is due to a combination of the finite numerical resolution and the imposed resistivity model. For constant η , increasing the numerical resolution (N) will eventually result in a behaviour of the solution that is independent of N . On the other hand, the current in the hyper-resistive case will continue to increase with N , with the physical structure having a length scale comparable to the numerical resolution. This can be seen by examining the growth of the dominant (z) component of \mathbf{J} for a run with double the resolution, shown by the dot-dashed line in Figure 3(b). The early evolution is very similar, though a higher current peak is eventually achieved after a longer period of localisation.

In a truly ideal evolution, it is expected that the current would increase indefinitely in time, although more and more of the energy associated with the disturbance would ‘escape’ down the spine [c.f. 20]. However, in a true physical case, no matter how small the resistivity, it will always become important eventually, once the current becomes sufficiently intense, and as a result some energy can be dissipated. This will occur all along the spine.

One very interesting question is how the maximum current depends on the resistivity. It is impossible here for us to use realistic resistive parameters appropriate for, e.g. the Solar corona, where the resistivity is typically of the order 10^{-14} . One crucial feature of any reconnection model is therefore whether the reconnection rate scales as some negative power of η —if so then it will typically

correspond to ‘slow’ reconnective behaviour in a realistic plasma. It is our intention to investigate this dependence in a subsequent paper in this series. It has furthermore recently been demonstrated [7, 22] that the plasma pressure (i.e. the value of the plasma- β) can have a profound effect on current scalings at 2D and 3D null points. This will also be investigated further in a later paper.

At a first glance, the type of tubular current structure described above is reminiscent of those found in the incompressible ‘spine reconnection’ solutions first described by [5] (in their case there exist two tubes in close proximity due to the assumed symmetry). In a general incompressible time-dependent case, a single tube of current is stretched out along the spine of the null, with the current being purely azimuthal within the tube (that is, directed parallel to the fan plane), rather than axial [23]. This is clearly rather different from the situation we have here, where the current is very close to being parallel to the spine. In addition, the incompressible spine reconnection solutions are associated with reconnection of field lines across the spine and fan (advection across the fan and diffusion across the spine), which we shall see below does not occur here.

One final important characteristic of the current evolution observed in our simulation is a non-linear coupling which may occur when the perturbation magnetic field is strong compared with the background field. As observed by [12], the main Alfvénic disturbance may also couple to a fast-mode wave which is attracted to the null point itself. This is, however, a fairly weak effect. [12] found that the coupling only existed in cases where the boundary driving was ramped sharply up from zero, and similarly we find that the strength of (and gradients in) the disturbance field must be very strong in order that the effect can be seen at all.

B. Plasma flow and field line behaviour

An examination of the plasma flow induced by the perturbation is of interest in itself, as well as in helping to determine what type of reconnective behaviour might result once a current sheet forms. It is perhaps not surprising that the rotational perturbation induces rotational plasma flows centred on the spine, in the xy -plane, as shown in Figure 4(a). The rotation is present within the ‘envelope’ of magnetic flux which was magnetically connected to the initial perturbation. Importantly, there is no plasma flow across either the spine or fan of the null. In fact, the direction of the plasma rotation in Figure 4(a) is somewhat complicated by reflections from the z -boundaries. Initially, the ingoing pulse generates clockwise flow (viewed from the z -boundaries) and the outgoing pulse anti-clockwise. In addition, once the ingoing pulse is reflected off the z -boundaries, it generates an additional region of anti-clockwise flow, which propagates in the negative z -direction. This occurs first at large radius within the flux envelope since this is where

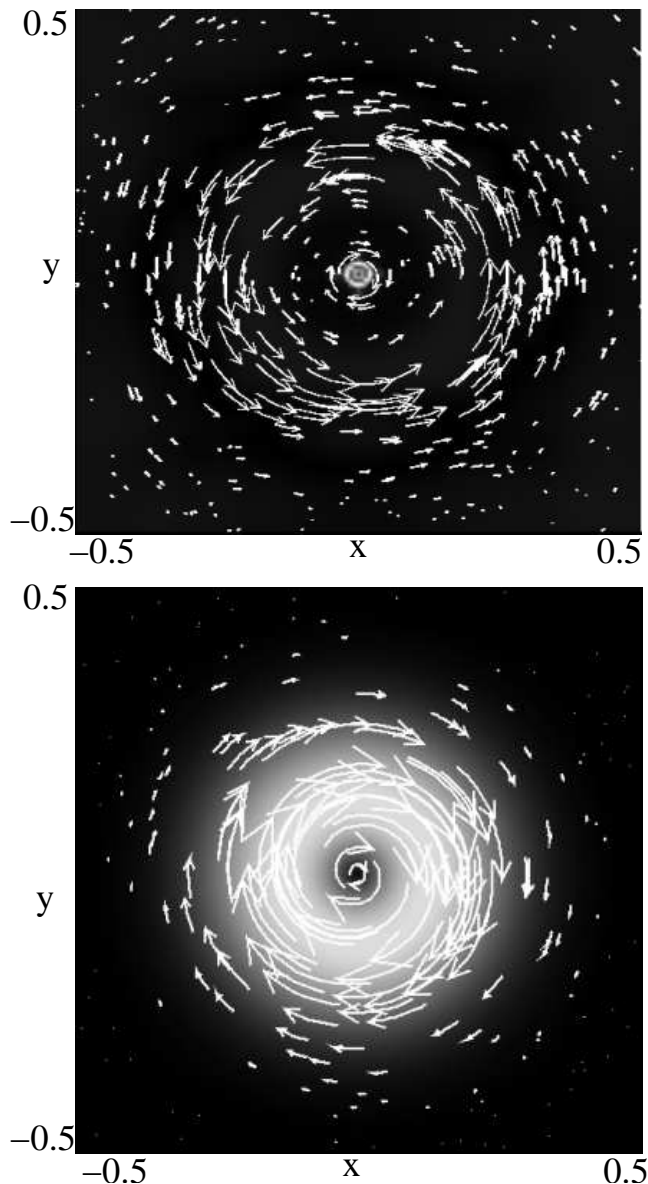


FIG. 4: Plasma flow in the plane $z \approx 0.05$, showing rotation centred on the spine (centre), for perturbations (a) rotation in the fan and (b) rotation about the spine. Pattern in other planes $z = z_0$ is similar, with only the r -localisation varying due to the hyperbolic nature of the flux envelope affected by the perturbation. The background shading shows the current modulus in the same plane in each case. Each image is at the time of maximum current, and the parameters are as in Figure 3 for (a), and for (b) $B_0 = 1$, $b_0 = \pm 0.1$, $\zeta_0 = \pm 0.2$, $\beta = 0.01$, $a_h = 0.06$, $b_h = 0.06$, $\eta = \eta_h$.

the reflection first occurs (see Figure 3). Thus, present in Figure 4(a) are the flow resulting from the ingoing pulse, and its reflection from the z -boundary.

As a result of this plasma flow, it seems unlikely that any reconnection involves field lines being advected across the separatrices, but rather a rotational mismatching would be expected. This is predicted by kinematic studies [25] when the current is parallel to the spine of

the null point. As shown in Figure 5, this is indeed the case. The plotted field lines are traced from two sets of trace-particles, which are initially connected (see Figure 5(a)). The first set of particles (from which the grey (blue online) field lines are traced) remain approximately in the ideal region, i.e. they are located far away from the null (near the fan plane) where currents remain weak. These field lines therefore show approximately the ideal behaviour, which is followed everywhere except close to the spine. (When the field lines pass close to the spine in the figure it is not possible to see the individual lines, due to the converging field structure.) The other set of particles is located close to the spine, such that they are eventually engulfed by the localising current. It can be seen that the corresponding field lines (black, red online) continually change their connections [see 26] in a rotational fashion as the current localises. Note that in the simulation pictured, a higher value of b_0 , and a constant resistivity ($\eta = 0.002$, implying a Lundquist number of order 500) have been used for illustrative purposes, since the diffusive region is larger for constant η than with the hyper-resistivity, and the effect of the diffusion is therefore easier to visualise.

C. Parallel electric field

It is well-known that a crucial indicator of 3D magnetic reconnection is the presence of an electric field component parallel to the magnetic field, E_{\parallel} [e.g. 30]. Examining an isosurface of E_{\parallel} , it is clear that non-ideal effects become important basically uniformly all along the spine (see Figure 6; taken a little before current maximum to limit appearance of boundary effects). Thus the reconnection seems to be associated with a spatially diffuse (at least in one dimension) region.

[24] showed that in the case of an isolated 3D null with current parallel to the spine, the rate of rotational flux mis-matching can be quantified by calculating the integrated parallel electric field (from one end of the diffusion region to the other) along the spine of the null (see also [15]). Care must be taken, however, in comparing our simulations with this kinematic result. The principal reason for this is that the result relies upon the assumption that the diffusion region is bounded in z , encompassing the null. Nonetheless, we find that $\Phi_s = \int E_{\parallel}$ (along the whole length of the spine within the domain) does indeed show a clear peak in time, indicating a maximum in the reconnection rate at the null, which occurs once the perturbation reaches the spine. That is, when the field gradients built up sufficiently that the current sheet begins to diffuse onto the spine, a parallel electric field can be seen to develop along it (see Figure 3). While the numbers we obtain here (Figure 3(b)) for E_{\parallel} are dependent on the resistivity model and/or value, the qualitative behaviour is not.

It is interesting to observe the close temporal correlation between the peak reconnection rate (Φ_s) at the

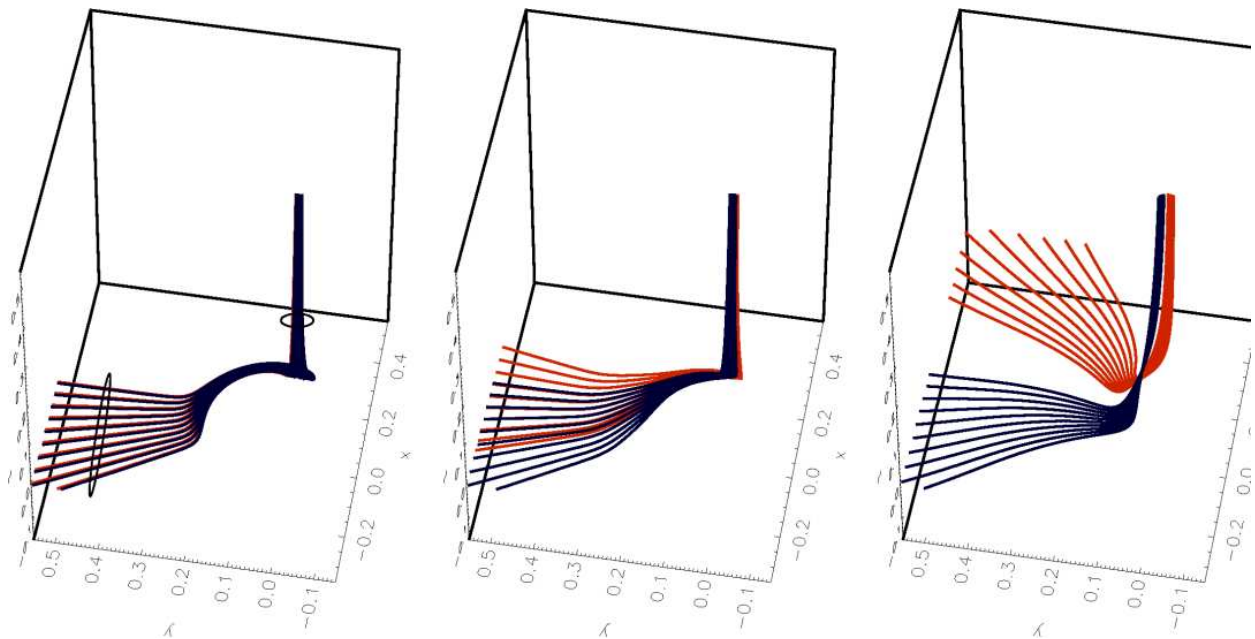


FIG. 5: Rotational slippage between two sets of magnetic field lines. The black loops enclose the two sets of fluid elements from which the field lines are traced. For parameters $B_0 = 1, b_0 = 3, R_{10} = 0.18, \beta = 0.01, a_h = 0.06, b_h = 0.06$ and constant $\eta = 0.002$. Again the total domain size is $1.5 \times 1.5 \times 2.5$. Times for the plots are $t = 0, 0.2, 0.9$.

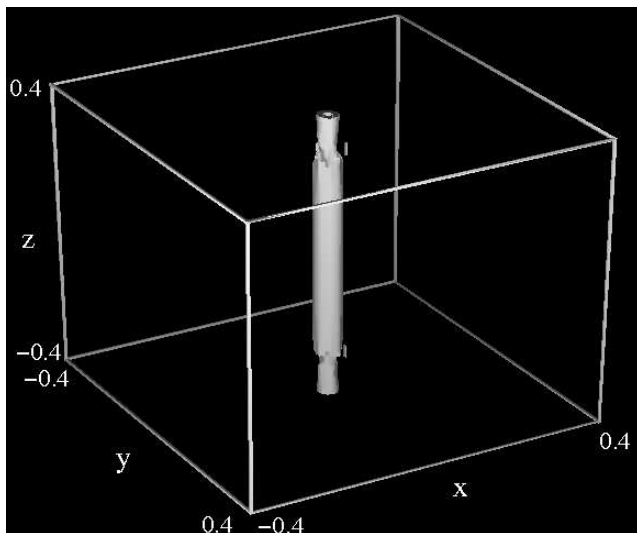


FIG. 6: Isosurface of E_{\parallel} resulting from a rotation in the fan plane, at 50% of its maximum, at $t = 2.16$ and for the same parameters as Figure 3.

null and the peak current. As mentioned previously, in the ideal limit we would expect J to grow indefinitely, due to the structure of the magnetic field in the vicinity of the null. Thus a current peak is also an indication (for our transient perturbations) that non-ideal processes have become important, allowing the stress in the field (here twist) to begin to significantly dissipate. With this type of perturbation, E_{\parallel} will also increase as the pulse approaches the spine due to the geometry of the mag-

netic field, which becomes increasingly B_z -dominated as one approaches the spine (at a given height, z).

IV. ROTATION ABOUT THE SPINE

For a rotation about the spine we may take a perturbation magnetic field of similar form to that used in the previous section. However, here we take ζ_0 non-zero and R_{10} to be zero. For perturbation above and below the fan plane, we superpose two disturbances of this form, with ζ_0 of opposite signs (Figures 1(c) and 2(c)). Whether the rotation is in the same or opposite sense on either side of the fan is determined by the relative signs of b_0 . We take $B_0 = 1, b_0 = \pm 0.1, \beta = 0.01, \zeta_0 = \pm 0.2, a_h = b_h = 0.06$. A thorough examination of the development of these types of perturbations has been carried out in a similar simulation, described by [12]. The one major difference between the two simulations is that they applied a driving velocity at the (line-tied) boundaries, whereas we perturb the magnetic field within the domain. We therefore only summarise the results here.

This time, as the perturbation evolves, it generates a current which spreads out in the fan plane as it approaches the null (see Figure 7(a)). However, the most important aspect of the current development is that there is once again no tendency for a focusing of the localisation towards the null itself. Regardless of whether the rotation has the same or opposite sense, there are inward and outward propagating disturbances, and in the ingoing disturbance \mathbf{J}_{xy} is amplified (Figure 7(b,d)). The outgoing pulse, which localises towards the spine in the

same way as was seen in Section III, shows a growth of J_z (Figure 7(c)). However, this time that current never reaches the null since the fan is not perturbed. There is also a relatively weak pulse of J_z which does propagate towards the fan plane and null (7(c)), as seen by [29], however, this is dominated by the strong \mathbf{J}_{xy} further out in the fan.

The fact that different current components are magnified in the ingoing and outgoing pulses is likely just a result of the geometry of the background field. In particular, moving inwards from a given point on the spine, $d/dx, d/dy$ decrease, while d/dz increases sharply as the fan is approached. Thus the current maximum occurs as the ingoing pulse steepens towards the fan. If the resistivity were zero, a fan current sheet (with infinite current density but of zero thickness) would be asymptotically approached. However, in our simulation, sufficiently steep gradients develop before the disturbances reach the fan, such that diffusion becomes important. This is one difference between our simulation and the driven case of [12], where the continual twisting at the boundaries drove the current right into the fan plane.

The plasma flow in this case is, as expected, of a rotational nature, with similar form to that found for rotation in the fan plane (and sense of rotation governed by the initial condition). A plot of the plasma velocity in the xy -plane demonstrating this is shown in Figure 4(b). Furthermore, the field line behaviour is found to be very similar to that shown in Figure 5.

As the disturbances here travel basically along \mathbf{B} and there is no flow and no magnetic connection between the two sides of the fan plane ($z > 0, z < 0$), there is essentially no difference for the case where the driving has the same sign on each side of the fan, except the sense of rotation. In addition, since the current is not driven right into the fan as in [12], there is no issue of the currents reinforcing or cancelling there as they found.

V. SHEAR OF THE FAN PLANE

The behaviour of shearing-type perturbations is very different to rotational ones. We first consider the case of a shear of the fan plane. The perturbation again takes the form described by Equation (7), where this time $\{b_i, b_j\} = \{b_x, b_z\}$ and $\zeta = y$. In addition we take $R_1 = \sqrt{(x-x_0)^2 + z^2}$, $\theta_1 = \tan^{-1}\left(\frac{z}{x-x_0}\right)$ and $R_{10} = \zeta_0 = 0$. This corresponds to a linear tube (of finite length) of azimuthal magnetic flux, whose axis lies along $x = x_0, z = 0$. We superimpose two such perturbations on our background null, with opposite signs of x_0 , as shown in Figure 1(b). The effect on the fan field lines is as if they have been ‘plucked’, in one direction in some region of the fan, and in the opposite direction in an opposite region (Figure 2(b)). We take (except where stated) $B_0 = 1$, $b_0 = 0.1$, $\beta = 0.01$, $x_0 = \pm 0.16$, $a_h = 0.06$, $b_h = 0.2$.

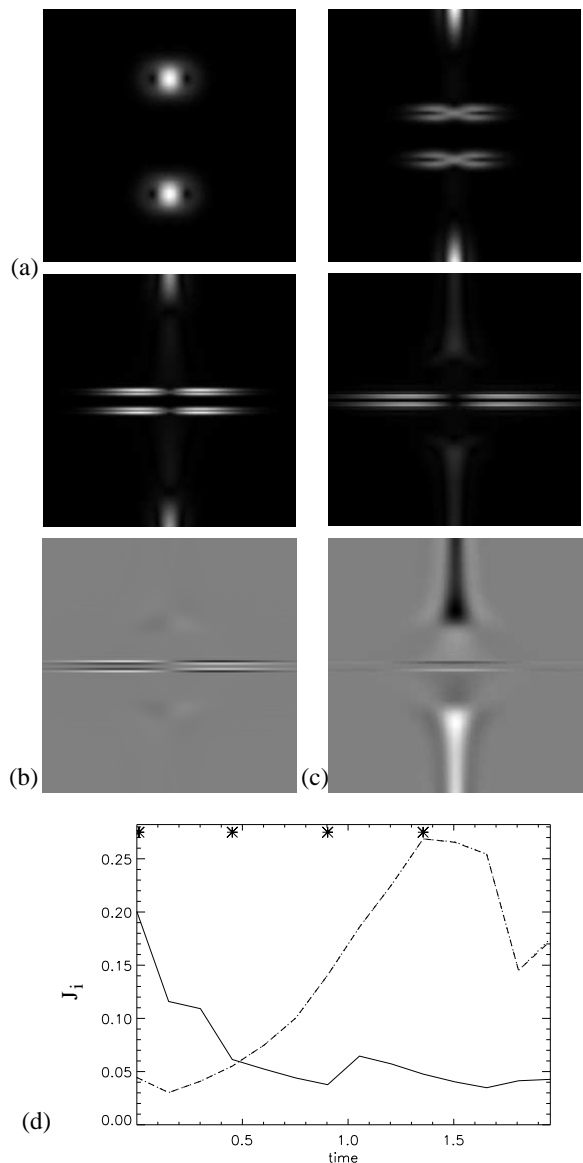


FIG. 7: For a rotation about the spine of opposite sense above and below the fan; (a) shaded images showing $|\mathbf{J}|$ in the $y = 0$ plane, for $[x, z] = [\pm 0.45, \pm 0.45]$, at times shown by the asterisks in (d) ($t = 0, 0.45, 0.9, 1.35$). (b) J_x and (c) J_z at $t = 1.35$ (time of maximum current). (d) Evolution of the maximum values of each current component in the inner half (in each direction) of the domain: J_x dotted, J_y dashed, J_z solid line. For domain size $1.5 \times 1.5 \times 1.5$ and parameters as in Figure 4(b).

A. Current and plasma flow

The crucial characteristic of the current development for a shear of the fan is that, while the disturbance propagates to some extent along the background field lines, there is additionally a strong focusing of the current (across the field) towards the null point itself (see Figure 8(a)). Note that again there is a fair degree of

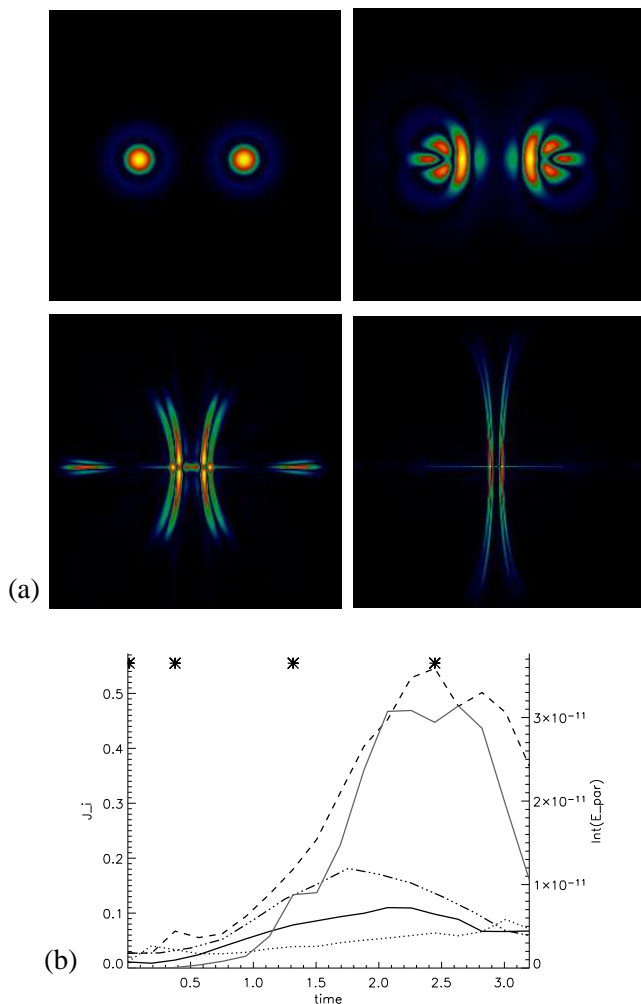


FIG. 8: For a shear of the fan; (a) shaded images showing $|\mathbf{J}|$ in the $y = 0$ plane, for $[x, z] = [\pm 0.45, \pm 0.45]$, at times marked by asterisks in (b) ($t = 0, 0.38, 1.32, 2.45$). (b) Evolution of the maximum values of each current component in the inner half (in each direction) of the domain: J_x dotted, J_y dashed, J_z solid black line. The grey line plots the integrated parallel electric field along the y -axis. For domain size $1.5 \times 1.5 \times 1.5$ and parameters $B_0 = 1, b_0 = 0.1, x_0 = \pm 0.16, \beta = 0.01, a_h = 0.06, b_h = 0.2, \eta = \eta_h$. The dot-dashed line shows J_y evolution in a run with the same parameters, but with $\eta = 5 \times 10^{-5}$, constant

structure to the localising current. This is because the disturbance was initiated by a divergence-free magnetic disturbance, in the form of a tube of magnetic field (see Figure 1(b)). Thus in fact three current concentrations, demarking field gradients at the front, middle and back end of the pulse are present. The components at the front and back end are necessarily of opposite sign (in J_y) to the strongest concentration in the middle, and the gradients of course go through zero between these regions, hence the appearance of three ‘pulses’ in $|\mathbf{J}|$. While the two outer regions initially join up to encircle the inner

concentration, this appearance is eventually lost due to the stretching of the structure in z .

It is evident from Figure 8(b) that the disturbance which focuses towards the null point is dominated by J_y , that is, the current orthogonal to the plane of the shear. Once again it is the resistivity which limits the growth of the current. In an ideal situation we would expect the current to continue to grow indefinitely, focusing at the null, where a good portion of the energy of the disturbance would be deposited, once resistive effects eventually become important.

As an explicit demonstration of the effect of our hyper-resistivity model, we re-run the simulation with η constant, taking $\eta = 5 \times 10^{-5}$ (in order to resolve all structures sufficiently). We find that the diffusion causes the peak current to be much lower, and occur much earlier when the perturbation is far less localised (see the dot-dashed line in Figure 8(b)). Qualitatively the current structure behaves very similarly—the same images as in Figure 8(a) look almost identical (when scaled by their individual maxima), except that in the final image (now long after current maximum), the current is not so strongly peaked near $z = 0$ as much of the perturbation has diffused away.

The presence of strong current at the null point directed parallel to the fan is expected to indicate the presence of more traditional reconnection-type flows. In the simplified kinematic model of [25], a stagnation-point flow, centred on the null, is present in the plane perpendicular to the shear. This flow transports magnetic flux across the spine and fan. Similarly here, at the time of maximum current (see Figure 9(a)), we indeed find strong plasma flow across the fan plane (originally $z = 0$), concentrated around the areas of maximum current. Away from the current concentrations as well, there is flow across the original locations of the spine and fan. However, it is not straightforward to determine whether magnetic reconnection is occurring at the null. This is because the flow may act to transport magnetic flux across the fan plane (magnetic reconnection), or it may simply act to advect the spine and fan in an ideal sense. It is therefore again of interest to examine the development of E_{\parallel} .

B. E_{\parallel} and reconnective behaviour

The presence of a parallel electric field denotes a breakdown of ideal behaviour, and so is crucial in determining whether magnetic reconnection occurs. We expect E_{\parallel} to be greatest in regions of high current, where the field lines lie in the direction of the current (since $E_{\parallel} = \eta J_{\parallel}$). Examining an isosurface of E_{\parallel} at current maximum (Figure 10), we see that in fact the highest concentrations are located (as expected) at regions of strong J , a little way from the y -axis (due to the structure of the initial disturbance). The most striking thing we see from Figure 10 is that in this case the regions in which E_{\parallel} develops are

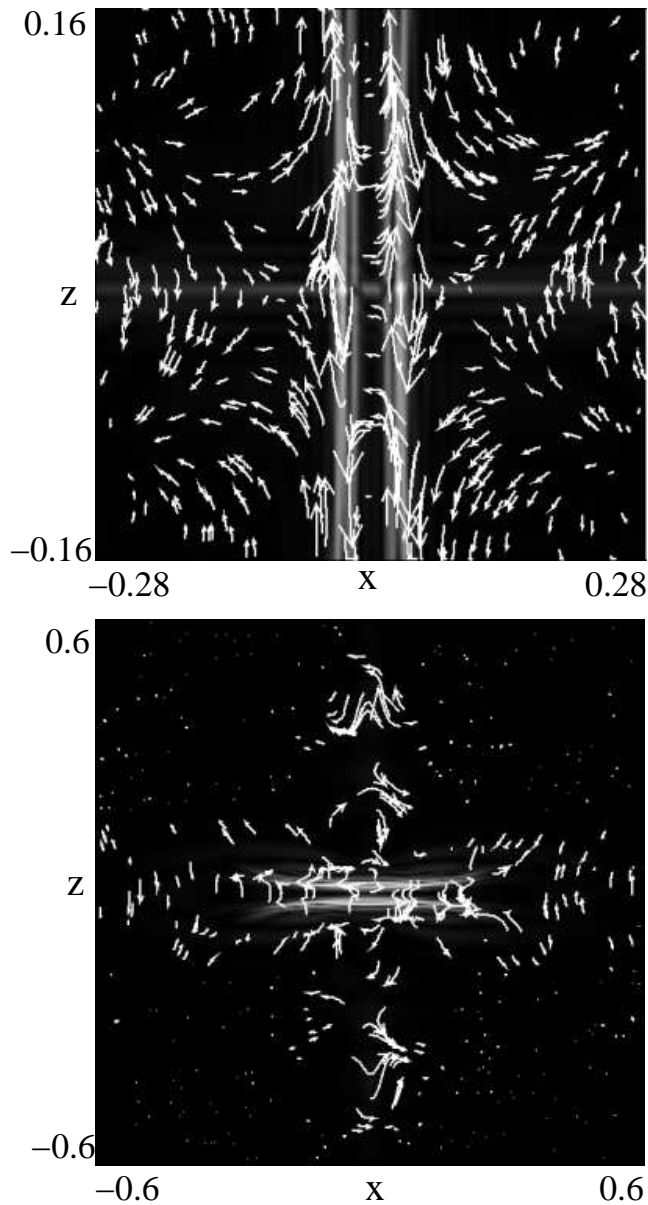


FIG. 9: (a) The plane $y = 0$, perpendicular to the shear, at time of maximum current ($t = 2.45$), for a shear of the fan. The arrows show the plasma flow, and the background shading the current modulus. Parameters as in Figure 8. (b) As (a), but for spine shear run ($t = 1.23$), for domain size $1.5 \times 1.5 \times 1.5$ and parameters $B_0 = 1, b_0 = 0.1, z_0 = \pm 0.2, \beta = 0.01, a_h = 0.05, b_h = 0.05, \eta = \eta_h$.

highly spatially localised in all directions. Hence reconnection processes are very local to the null itself. While this localisation is not quite so extreme in runs with constant resistivity, the basic structure is the same.

For an isolated null with fan-aligned current, surrounded by a localised non-ideal region, the integral of E_{\parallel} along the magnetic field line in the fan plane which is directed along \mathbf{J} can be shown to give an exact measure of the rate of flux transfer across the fan, where the integral

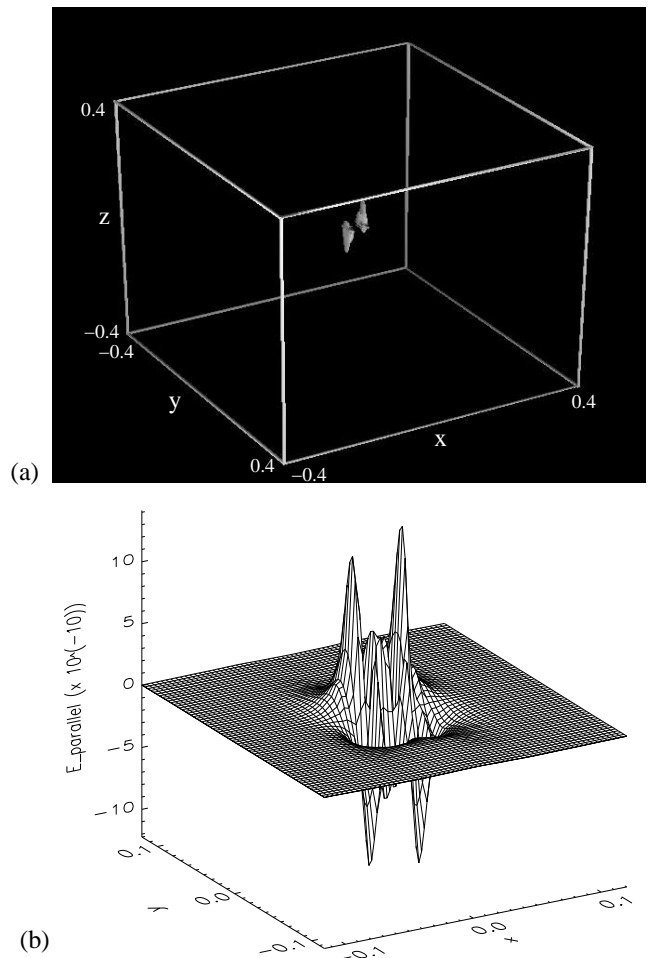


FIG. 10: For a shear of the fan plane, (a) isosurface of E_{\parallel} at 25% of its maximum and (b) surface of E_{\parallel} in the $z = 0$ plane (interpolated onto a uniform grid), both at $t = 2.45$ (current maximum), for the same parameters as in Figure 8.

is taken from one side of the diffusion region (assumed spatially localised at the null) to the other [25]. Thus, a non-zero value for $\Phi_f = \int E_{\parallel} ds$ along a fan field line threading the diffusion region implies that magnetic flux is transferred across the separatrix (fan) plane, even in the ideal region, and thus demonstrates that reconnection is occurring at the null. Performing such an integration, $\Phi_f = \int_{x=z=0} E_{\parallel} ds$, we find a parallel electric field does indeed develop, a strong indicator that some reconnective process is taking place. Note that here again the peaks of Φ_f and J_{max} are closely correlated.

In fact, when Φ_f reaches its temporal maximum, the spatial maximum of E_{\parallel} is still some distance from the y -axis (see Figure 10). In the fan plane, the maxima actually occur on field lines which lie approximately along $x = \pm y$. The reason for this is as follows. The electric field, like \mathbf{J} , is directed largely in the \hat{y} direction perpendicular to the shear, and is uni-directional through the null. Thus $E_{\parallel} \approx 0$ on the x -axis, and $E_{\parallel} > 0$ for $y > 0, E_{\parallel} < 0$ for $y < 0$ (see Figure 10(b)). If the per-

turbation were to extend azimuthally around the entire fan plane, we would expect the maximum and minimum of E_{\parallel} to be on the y -axis. Such an azimuthally symmetric perturbation could be envisaged by considering a field localised within the torus of Figure 1(a) which is purely poloidal rather than toroidal, and which has a $\cos(\theta)$ multiplying factor (where $\theta = \tan^{-1}(y/x)$). However, since the chosen shear has a finite azimuthal extent, maxima and minima of E_{\parallel} are found off the y -axis. Therefore, by comparison with [25], we expect a better measure of the rate of flux transfer across the fan to be given by $\Phi_f' = \int_{x=y, z=z_{fan}} E_{\parallel} ds$, by symmetry, giving the maximal value of Φ_f . This quantity shows a similar qualitative evolution to that of Φ_f plotted in Figure 8(b).

The nature of the magnetic reconnection associated with E_{\parallel} can again be examined by tracing field lines from trace particles which are initially magnetically connected. A typical evolution for an appropriately chosen set of field lines is shown in Figure 11. It is clear that the chosen plasma elements change their connections in such a way as to suggest a transport of magnetic flux across both the spine and fan of the null. Specifically, grey field lines (green online, traced from ‘non-ideal’ footpoints located near the fan plane, between the initial perturbation and the null) are transported across the fan plane (from above to below), whereas black field lines (red online, traced from ‘ideal’ plasma elements located far up the spine) are advected across the spine.

VI. SHEARING THE SPINE

To complete the picture we finally consider a perturbation which shears the spine of the null point. The disturbance takes the form given by Equation (7), with $\{b_i, b_j\} = \{b_x, b_z\}$, $\zeta = y$, $R_1 = \sqrt{x^2 + (z - z_0)^2}$, $\theta_1 = \tan^{-1}\left(\frac{z - z_0}{x}\right)$ and $R_{10} = \zeta_0 = 0$. Again two such disturbance fields are superimposed, with opposite signs of z_0 (see Figure 1(d)). The effect on the spine field line is as if it has been locally ‘plucked’, in opposite directions above and below the null (see Figure 2(d)). We take (except where stated) $B_0 = 1$, $b_0 = 0.1$, $\beta = 0.01$, $z_0 = \pm 0.2$, $a_h = b_h = 0.05$.

The resulting current evolution in the plane perpendicular to the shear is shown in Figure 12, from which it can be seen that the inward-propagating component of the disturbance is again attracted towards the null point, as in the case of a shear of the fan. Although both J_x and J_y are magnified during this localisation, in fact $\mathbf{J} = J_y$ at the null point itself. That is, the current which develops at the null is again parallel to the fan, perpendicular to the plane of shear.

As before, a plot of the plasma velocity in the plane perpendicular to the shear (see Figure 9(b)), suggests flow across the spine and fan, although again it is hard to say whether the flow actually crosses the spine and fan, or merely ideally advects them. In addition, there is also some complicated (and relatively strong) flow across

the spine within the region of the localising current concentration.

Some representative field lines are plotted in Figure 13. Field lines traced from plasma elements initially located near the spine (black, green online) are transported back and forth across the spine, since these plasma elements are engulfed by the current concentration. The grey field lines (red online), however, are traced from plasma elements which stay forever in the ‘ideal’ region, far out along the fan plane, and are clearly advected across the separatrix surface. In fact, the behaviour of the null in response to the perturbation is similar to the case where the fan plane is sheared. In each case, the current is peaked at the null itself, and field lines reconnect in a manner similar to the traditional 2D picture, in the plane of the shear.

VII. SUMMARY

The behaviour of perturbations in the vicinity of a potential 3D magnetic null point has been investigated via resistive magnetohydrodynamic simulations. Disturbances which affect the null point must deform the field in the vicinity of either the spine or the fan of the null. A typical such disturbance may be constructed using a combination of shears and rotations, and hence we considered four basic possibilities—namely shear of the fan or spine, and rotation of the fan or about the spine. It should be pointed out that we consider a case with no initial ‘background’ flow, that is there is no flow through our boundaries, and therefore we do not compare with strongly driven flux pile-up models.

We have found that rotational types of perturbations tend to lead to current accumulation in the vicinity of the field lines which asymptotically approach (or recede from) the null point, that is the spine and fan field lines. The disturbances behave in a way which is essentially Alfvénic, propagating along the background field lines. Thus, (apart from a weak non-linear wave-mode coupling) there is no preferential growth of current at the null point itself. Near the null, the current accumulates along the spine when the rotations disturb the fan plane, while rotations about the spine lead to currents in the location of the fan near the null. Such diffuse currents, extending along the separatrix surfaces, have been predicted in incompressible analytic models [5, 6], although the form we find for the current sheets is somewhat different. The plasma flows and field line reconnection associated with these currents is of a rotational nature, as predicted by [24].

By contrast, when the spine or fan of the null is subjected to a shearing perturbation, there is a strong current growth which is localised at the null point itself. This is achieved by propagation of the disturbance across the background magnetic field lines, suggesting that the dominant wave mode associated with the disturbance is a fast mode. This behaviour agrees with the results of

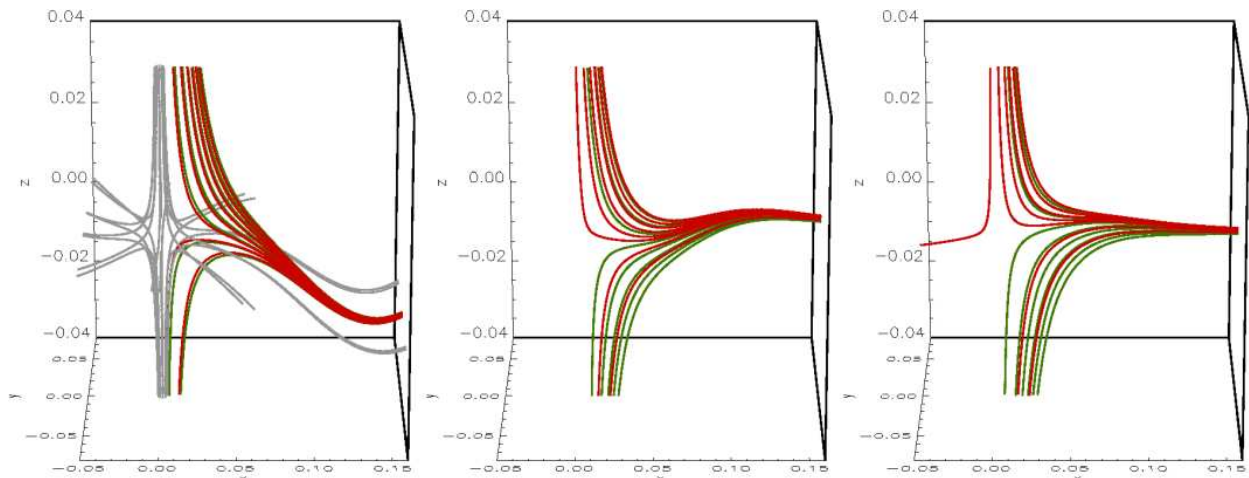


FIG. 11: Evolution of two initially connected sets of field lines when the fan is sheared. One set are traced from plasma elements which remain always in the ideal region far up the spine (black, red online) and is advected across the spine. The other (grey, green online, traced from plasma elements initially within the black loop) are traced from plasma elements near the $z = 0$ plane and are transported across the fan. Parameters as in Figure 8, but $b_0 = 3, \eta$ constant = 0.002. The dashed field lines in the first image indicate the initial location of the spine and fan. Times for the images are $t = 0, 0.8, 1.6$

[29], and is consistent also with the work of [22], who found singular current sheets to result at a 3D null point in an ideal line-tied relaxation when a shear was applied to spine or fan. The current which develops at the null is dominated by the component in the direction perpendicular to the plane of shear. The resulting plasma flow has a stagnation-point structure. It is in general very difficult to say from such simulations definitively that the plasma actually crosses the spine and fan. In the ideal region the flow advects field lines ideally, however it may still cross the spine or fan, if the spine and fan field lines change their identities (where now a field line is identified by plasma elements which lie on it in the ideal region) in time via magnetic reconnection (as in steady-state 2D reconnection). Despite this difficulty, by comparison with kinematic models [25], the non-zero integrated parallel electric field which develops along fan field lines is a strong indicator of flux transfer across at least the fan. The magnetic field line evolution shows a reconnection of field lines through/around the spine and across the fan plane, as in the ‘spine reconnection’ and ‘fan reconnection’ of [28]. The transport of magnetic flux across the fan plane is a particularly important property, as it is a separatrix surface of the magnetic field. The behaviour of shearing perturbations is further in agreement with the kinematic predictions of [25].

Finally, we investigated the existence and behaviour of parallel electric fields within the simulations. In each case investigated, in order to halt the indefinite growth of \mathbf{J} , resistive effects become important, as evidenced by the development of E_{\parallel} . In the case of rotational pertur-

bations, the spatial profile of E_{\parallel} (as with \mathbf{J}), is spread out either along the spine or the fan of the null. For shear perturbations, however, E_{\parallel} tends to be strongly localised at the null point itself. Such parallel electric fields can be shown to give a physically meaningful measure of the reconnection rate at a 3D null [24, 25] (though direct analogy with these kinematic results is not completely straightforward here). Finally, the dependence of the behaviour of the system, and the scaling of the peak currents and reconnection rate, on resistivity, plasma- β and the isotropy of the background null point are all important issues, as is the energetics of the reconnection process. These will be left for exploration in a future paper.

Acknowledgments

The authors would like to acknowledge helpful discussions with A. Bhattacharjee and I. J. D. Craig. D. P. was funded by the Department of Energy, Grant No. DE-FG02-05ER54832, by the National Science Foundation, Grant No. ATM-0422764, and in the initial stages of this work by the Marsden Fund, grant no. 02-UOW-050 MIS. K. G. was supported by the Carlsberg Foundation in the form of a fellowship. Computations were performed on the Zaphod Beowulf cluster which was in part funded by the Major Research Instrumentation program of the National Science Foundation under grant ATM-0420905.

[1] Brown, D. S. and Priest, E. R. (2000). Topological differences and similarities between force-free and potential

models of coronal magnetic fields. *Solar Phys.*, 194:197–

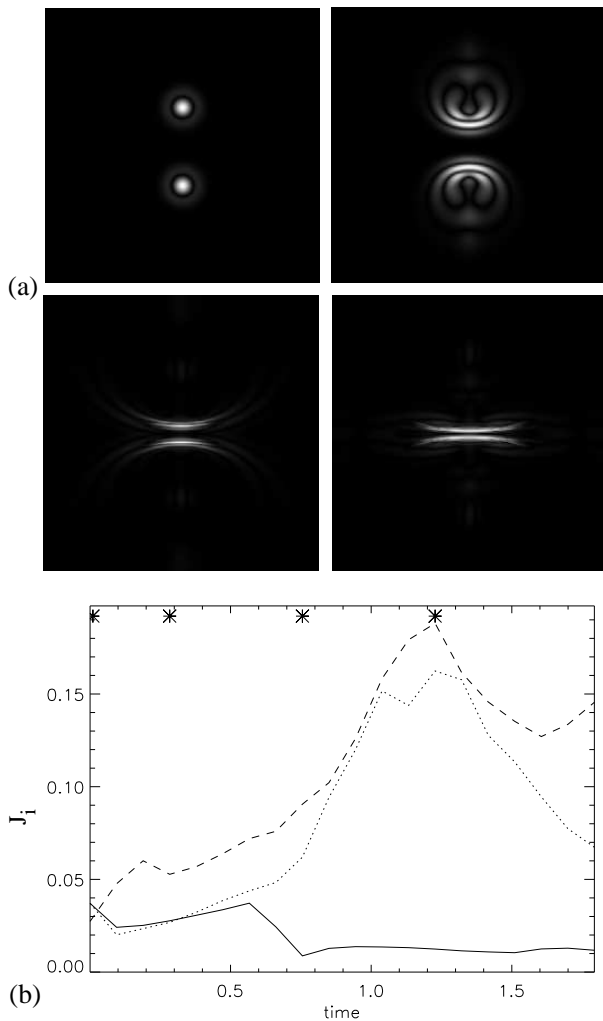


FIG. 12: For a shear of the spine; (a) shaded images showing $|\mathbf{J}|$ in the $y = 0$ plane, for $[x, z] = [\pm 0.75, \pm 0.75]$, at times marked by asterisks in (b) ($t = 0, 0.28, 0.76, 1.23$). (b) Evolution of the maximum values of each current component in the inner half (in each direction) of the domain: J_x dotted, J_y dashed, J_z solid black line. Parameters as in Figure 9(b).

204.

- [2] Brown, D. S. and Priest, E. R. (2001). The topological behaviour of 3D null points in the sun's corona. *Astron. Astrophys.*, 367:339–346.
- [3] Bulanov, S. V. and Olshanetsky, M. A. (1984). Magnetic collapse near zero points of the magnetic field. *Phys. Lett.*, 100:35–38.
- [4] Close, R. M., Parnell, C. E., and Priest, E. R. (2004). Separators in 3d quiet-sun magnetic fields. *Solar Phys.*, 225:21–46.
- [5] Craig, I. J. D. and Fabling, R. B. (1996). Exact solutions for steady-state, spine, and fan magnetic reconnection. *Astrophys. J.*, 462:969–976.
- [6] Craig, I. J. D., Fabling, R. B., Henton, S. M., and Rickard, G. J. (1995). An exact solution for steady state magnetic reconnection in three dimensions. *Astrophys. J. Lett.*, 455:L197–L199.
- [7] Craig, I. J. D. and Litvinenko, Y. E. (2005). Current singularities in planar magnetic X-points of finite compressibility. *Phys. Plasmas*, 12:032301.
- [8] Craig, I. J. D. and McClymont, A. N. M. (1993). Linear theory of fast reconnection at an X-type neutral point. *Astrophys. J.*, 405:207–215.
- [9] Fletcher, L., Metcalf, T. R., Alexander, D., Brown, D. S., and Ryder, L. A. (2001). Evidence for the flare trigger site and three-dimensional reconnection in multi-wavelength observations of a solar flare. *Astrophys. J.*, 554:451–463.
- [10] Fukao, S., Ugai, M., and Tsuda, T. (1975). Topological study of magnetic field near a neutral point. *Rep. Ion. Sp. Res. Japan*, 29:133–139.
- [11] Galsgaard, K. and Nordlund, A. (1997). Heating and activity of the solar corona: 3. Dynamics of a low beta plasma with 3D null points. *J. Geophys. Res.*, 102:231–248.
- [12] Galsgaard, K., Priest, E. R., and Titov, V. S. (2003). Numerical experiments on wave propagation towards a 3D null point due to rotational motions. *J. Geophys. Res. Space*, 108:SSH 10–1.
- [13] Galsgaard, K., Reddy, R. V., and Rickard, G. J. (1997). Energy release sites in magnetic fields containing single or multiple nulls. *Solar Phys.*, 176:299–325.
- [14] Hassam, A. B. (1992). Reconnection of stressed magnetic fields. *Astrophys. J.*, 399:159–163.
- [15] Hornig, G. and Priest, E. R. (2003). Evolution of magnetic flux in an isolated reconnection process. *Phys. Plasmas*, 10(7):2712–1721.
- [16] Lau, Y. T. and Finn, J. M. (1990). Three dimensional kinematic reconnection in the presence of field nulls and closed field lines. *Astrophys. J.*, 350:672–691.
- [17] Longcope, D. W. (1996). Topology and current ribbons: A model for current, reconnection and flaring in a complex, evolving corona. *Solar Phys.*, 169:91–121.
- [18] Longcope, D. W., Brown, D. S., and Priest, E. R. (2003). On the distribution of magnetic null points above the solar photosphere. *Phys. Plasmas*, 10:3321–3334.
- [19] Longcope, D. W. and Cowley, S. C. (1996). Current sheet formation along three-dimensional magnetic separators. *Phys. Plasmas*, 3:2885–2897.
- [20] McLaughlin, J. A. and Hood, A. W. (2004). Mhd wave propagation in the neighbourhood of a two-dimensional null point. *Astron. Astrophys.*, 420:1129–1140.
- [21] Nordlund, A. and Galsgaard, K. (1997). A 3d mhd code for parallel computers. Technical report, Astronomical Observatory, Copenhagen University.
- [22] Pontin, D. I. and Craig, I. J. D. (2005). Current singularities at finitely compressible three-dimensional magnetic null points. *Phys. Plasmas*, 12:072112.
- [23] Pontin, D. I. and Craig, I. J. D. (2006). Dynamic 3D reconnection in a separator geometry with two null points. *Astrophys. J.*, 642:568–578.
- [24] Pontin, D. I., Hornig, G., and Priest, E. R. (2004). Kinematic reconnection at a magnetic null point: Spine-aligned current. *Geophys. Astrophys. Fluid Dynamics*, 98:407–428.
- [25] Pontin, D. I., Hornig, G., and Priest, E. R. (2005). Kinematic reconnection at a magnetic null point: Fan-aligned current. *Geophys. Astrophys. Fluid Dynamics*, 99:77–93.
- [26] Priest, E. R., Hornig, G., and Pontin, D. I. (2003). On the nature of three-dimensional magnetic reconnection. *J. Geophys. Res.*, 108(A7):SSH6–1.

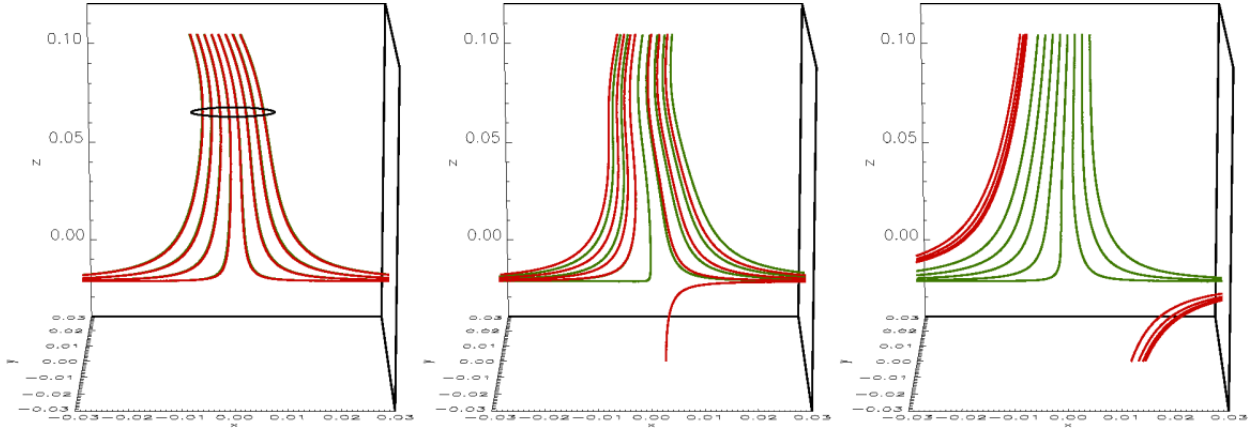


FIG. 13: For a shear of the spine, evolution of field lines traced from plasma elements near the spine (black, green online, ‘non-ideal’, traced from plasma elements initially located within the black ring in the first image) and near the fan (grey, red online, ‘ideal’). Parameters as in Figure 9(b), except that $b_0 = 3$, $\eta = 0.002$ constant. Images are at times $t = 0, 0.25, 0.7$.

- [27] Priest, E. R., Longcope, D. W., and Heyvaerts, J. F. (2005). Coronal heating at separators and separatrices. *Astrophys. J.*, 624:1057–1071.
- [28] Priest, E. R. and Titov, V. S. (1996). Magnetic reconnection at three-dimensional null points. *Phil. Trans. R. Soc. Lond. A*, 354:2951–2992.
- [29] Rickard, G. J. and Titov, V. S. (1996). Current accumulation at a three-dimensional magnetic null. *Astrophys. J.*, 472:840–852.
- [30] Schindler, K., Hesse, M., and Birn, J. (1988). General magnetic reconnection, parallel electric fields, and helicity. *J. Geophys. Res.*, 93(A6):5547–5557.
- [31] Schrijver, C. J. and Title, A. M. (2002). The topology of a mixed-polarity potential field, and inferences for the heating of the quiet solar corona. *Solar Phys.*, 207:223–240.
- [32] Siscoe, G. L. (1988). *Physics of Space Plasmas*, pages 3–78. Scientific, Cambridge, Mass.
- [33] Xiao, C. J., Wang, X. G., Pu, Z. Y., Zhao, H., Wang, J. X., Ma, Z. W., Fu, S. Y., Kivelson, M. G., Liu, Z. X., Zong, Q. G., Glassmeier, G. H., Balogh, A., Korth, A., Reme, H., and Escoubet, C. P. (2006). In situ evidence for the structure of the magnetic null in a 3d reconnection event in the earths magnetotail. *Nature*, 2:478–483.